Analysis of resolution enhancement through microsphere-assisted interferometry in the 3D spatial frequency domain

Lucie Hüser[a] and Peter Lehmann[a]

[a]University of Kassel, EECS, Measurement Technology Group, Wilhelmshöher Allee 71, 34121 Kassel, Germany

ABSTRACT

In optical metrology various approaches have been made in order to push the physical limitations of lateral resolution in microscopic and interferometric devices. Microsphere-assisted interferometry enables the measurement of structures well below Abbe's resolution limit. In order to give an approach for analyzing the obtained measurement data, this study shows the transfer behavior in the three-dimensional spatial frequency domain. With the construction of an Ewald sphere further insight into the role of microspheres in the imaging process can be obtained. For improved analysis, selective illumination is applied to the select those parts of the field of view where the microsphere is located. Further improvement is achieved by appropriate windowing of the measurement data.

Keywords: Interference microscopy, microsphere assistance, resolution enhancement

1. INTRODUCTION

In current research and industrial process control, the demand for high-precision measuring systems steadily increases. Due to applications in biology or in the quality control of semiconductor devices, there is a need for measurement technology that can be used contactless, marker-free and fast for the detection of laterally extended structures. Optical measurement technology using interference microscopy fulfills these requirements, as 3D topographies can be captured rapidly without any special preparation. By analyzing the phase of interferometric measurement data, it is possible to achieve an axial resolution of the topography data in the single-digit nanometer range.[1] A disadvantage, however, is the physical limitation of the lateral resolution found by Ernst Abbe. For spatially incoherent illumination this is given by[2]

$$d_{min} = 0.5\,\frac{\lambda}{n_i \cdot \sin\theta_{max}} = 0.5\,\frac{\lambda}{\mathrm{NA}}, \tag{1}$$

where λ represents the illumination wavelength, n_i the refractive index of the surrounding medium and θ_{max} the maximum angle of incidence with respect to the optical axis that can still be captured by the microscope objective lens.

Overcoming Abbe's resolution limit and thus making smaller lateral dimensions accessible for interference microscopy is a research topic of great interest. In 2011, Wang et al.[3] presented a method in which microspheres applied to the measurement object in the near field ensure a resolution improvement in brightfield light microscopy. Shortly afterwards, this approach was confirmed by other working groups. Darafsheh et al.[4] show a super-resolving behavior for liquid-immersed microspheres and point out the advantages over other techniques.[5] Applications in research are shown by the imaging process of adenoviruses.[6] Microsphere assistance has also found successful application in other optical measuring systems such as confocal microscopy.[7] Investigations on the illumination conditions[8] with microsphere support and dark field microscopy were carried out.[9]

Further author information: (Send correspondence to Lucie Hüser)
L. H.: E-mail: lucie.hueser@uni-kassel.de, Phone: +49 561 804-6505
P. L.: E-mail: p.lehmann@uni-kassel.de, Phone: +49 561 804-6313

Optical Measurement Systems for Industrial Inspection XII, edited by Peter Lehmann, Wolfgang Osten, Armando Albertazzi Gonçalves, Proc. of SPIE Vol. 11782, 117820R
© 2021 SPIE · CCC code: 0277-786X/21/$21 · doi: 10.1117/12.2593296

After a successful application of this method in conventional microscopy, it was also successfully applied in white light interference microscopy.[10] For further interferometric measuring systems it was shown that with the support of microspheres applied in the near-field it is possible to extend the resolution limit for interferometric height profile measurements.[11,12] Numerical apertures in the range of 0.3 to 0.85 were used, enabling access to high-frequency image information through the improvement of the optical resolution. Thus, high-spatial-frequency surface height information could be accessed by interferometers in optical measurement technology.[13–15]

To explain the effect of the resolution improvement, it is often referred to photonic nanojets.[16] These describe the focus of the light that is created on the backside of a microsphere illuminated with a plane wave. On the scale of microspheres, this focus is characterized by its high intensity and narrow waist.[17] Numerous papers have been published, studying the behavior and engineering of photonic nanojets.[18,19] In this context also the role of evanescent waves and whispering gallery modes have been discussed.[20] However, in conventional brightfield and in interference microscopy commonly incoherent Koehler illumination is applied, and thus microspheres are not illuminated by plane waves. Furthermore, the effects of differently structured concentric lighting of microspheres were examined.[21] Nevertheless, till now there is no complete and widely accepted explanation of the super-resolving behavior of microspheres in microscopy and interferometry. For this reason, further analysis of the underlying physical principles is necessary. Analyzing interferometric measuring systems in the three-dimensional (3D) spatial frequency domain gives insight into the relevant transfer characteristics. It allows conclusions to be drawn on the behavior and the properties of the system. Sheppard et al.[22] introduced a model which represents the imaging process of confocal microscopes in the 3D spatial frequency domain. This model was extended in further publications on confocal microscopy[23–25] and later introduced as the foil model in coherence scanning interferometry.[25–27] We recently extended this model by treating the reference mirror in the same way as the object's surface.[28]

By analyzing the interferometric measurement data in the 3D spatial frequency domain, the influence of microspheres on the transfer behavior of the optical system could already be shown.[29] In the following, the transfer characteristics of a high-resolution Linnik interferometer with microsphere assistance is pointed out in the 3D spatial frequency domain for different laterally extended periodic grating structures. Furthermore, it will be discussed how the transfer behavior of the interferometer with microsphere assistance performs when a selective circular and annular illumination of the image area covered by the microsphere is applied. First, the experimental setup is discussed, then the methodology for analyzing the measurement data in the spatial frequency domain is presented. Finally, results of the 3D spatial frequency domain analysis of measurement data are shown.

2. EXPERIMENTAL SETUP

A Linnik interferometer setup is used to record interference images at certain height positions during a depth scan, resulting in the so-called 3D image stack. From these measurement data the 3D height information is reconstructed for each camera pixel by appropriate signal processing algorithms finally leading to the measured 3D surface topography. The Linnik interferometer setup is equipped with two microscope objectives put in the measuring and the reference arm, respectively. We use two high-resolution microscope objective lenses with 100x magnification and an NA of 0.9 made by Olympus. The camera used for image acquisition is a scientific CMOS camera from Hamamatsu. For the illumination an LED from LUXEON ($\lambda = 460\,\mathrm{nm}$) as well as a Digital Micromirror Device (DMD) are built in the illumination path of the setup to enable selective circular and annular illumination of the measurement object. A schematic drawing of the experimental setup and a photograph are shown in Figure 1.

The interferometric data acquisition is done by performing the depth scan using a precision piezo stage (Physik Instrumente), where the object is put on. A small height step of typically 20 nm between two consecutive image acquisitions by the camera is chosen in order to get a good signal in the frequency range of the interference pattern. The resulting image stack can then be analyzed pixel by pixel using envelope and phase evaluation algorithms in order to reconstruct the 3D topography of the surface of the measurement object.[1]

When using microspheres in the near field of the measured surface, the spheres are first put on the measurement object in a liquid emulsion for practical reasons. After the liquid has evaporated, the measurement

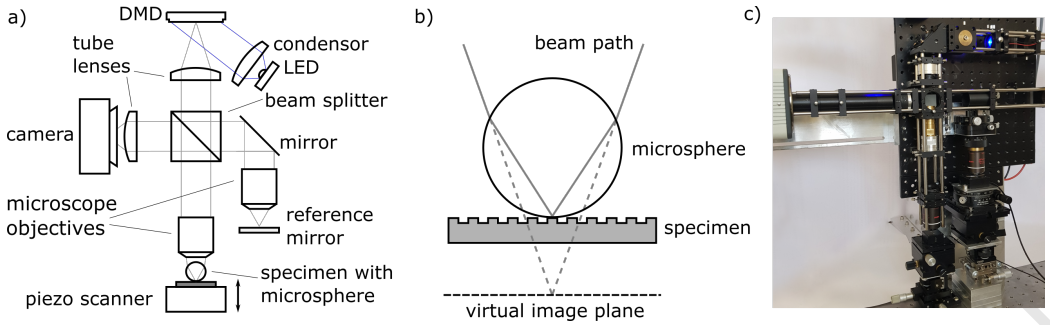

Figure 1. a) Schematic drawing of the experimental Linnik interferometer setup; For simplification purposes the illumination path (blue) is only shown for illumination of the DMD; b) Enlarged schematic drawing of the near-field measurement setup of a specimen with a microsphere on top creating a virtual image plane; c) Photograph of the experimental setup in the laboratory.

can be carried out. The microspheres used throughout the presented experiments are SiO_2 microspheres with a diameter of 5-15 µm made by micromod Partikeltechnologie GmbH. With the application of microspheres in the imaging path, a shift of the focus occurs and creates a virtual image plane as it is sketched in Fig. 1b.

3. ANALYSIS IN THE 3D SPATIAL FREQUENCY DOMAIN

In order to understand the relevance of an analysis of interferometric measurement data in the spatial frequency domain, it is helpful to first analyze the origin of the Abbe criterion mentioned in equation 1. It can be derived from the diffraction of an incident plane wave with the wave vector $\vec{k}_{in}$ at a grating structure, which is periodic in one lateral dimension. Diffraction maxima occur in the Fourier plane of the optical imaging system. The positions of these maxima on the lateral spatial frequency axis is reciprocal to the period length of the illuminated grating. For incoherent illumination, the Abbe limit denotes the period length at which at least one of the two first order diffraction maxima (directly connected to scattering angle, the scattering wave vector k_s includes with the optical axis) can still be captured by the microscope objective. This maximum scattering angle is limited by the numerical aperture of the objective lens. This directly leads to the Abbe criterion. The wave vectors can be described as follows:[28,30]

$$\vec{k}_{in} = k_0 \begin{pmatrix} \sin(\theta_{in})\cos(\varphi_{in}) \\ \sin(\theta_{in})\sin(\varphi_{in}) \\ -\cos(\theta_{in}) \end{pmatrix} \quad \text{and} \quad \vec{k}_s = k_0 \begin{pmatrix} \sin(\theta_s)\cos(\varphi_s) \\ \sin(\theta_s)\sin(\varphi_s) \\ \cos(\theta_s) \end{pmatrix}, \tag{2}$$

where $k_0 = 2\pi/\lambda$, θ_{in} and θ_s are the polar incident and scattering angles, and φ_{in} and φ_s the azimuthal out-of-plane angles with respect to the xz-plane, respectively. When considering interferometric measurement data and the transfer behavior of optical systems in the spatial frequency domain, the data can be analyzed in the $q_{x/y}q_z$-plane.[28,31] The distribution of the electromagnetic field components depends on the incident and scattered waves. This results in the vector $\vec{q} = \vec{k}_s - \vec{k}_{in}$, which represents the relationship between incident and diffracted or scattered light in the spatial frequency domain. For a one-dimensional grating, which is translational invariant with respect to the y-coordinate, this leads to

$$\vec{q} = k_0 \begin{pmatrix} \sin(\theta_s)\cos(\varphi_s) - \sin(\theta_{in})\cos(\varphi_{in}) \\ 0 \\ \cos(\theta_{in}) + \cos(\varphi_s) \end{pmatrix} \tag{3}$$

Interferometric measurement data, which is analyzed in the 3D spatial frequency domain, can potentially cover a volume across all possible frequency components that correspond to the construction of an Ewald sphere. The limitation of this volume in the x/y-direction is determined by the maximum possible angles of incidence and scattering, which are directly related to the numerical aperture of the objective. In the direction of the scan axis z, a range from $q_z = \frac{4\pi}{\lambda}\sqrt{1-NA^2}$ to $q_z = 4\pi/\lambda$ is covered. The behavior of the wave vectors is shown in

Figure 2a) and b), the resulting construction in the spatial frequency domain in relation to the $q_x q_z$ plane in Figure 2c) and d).

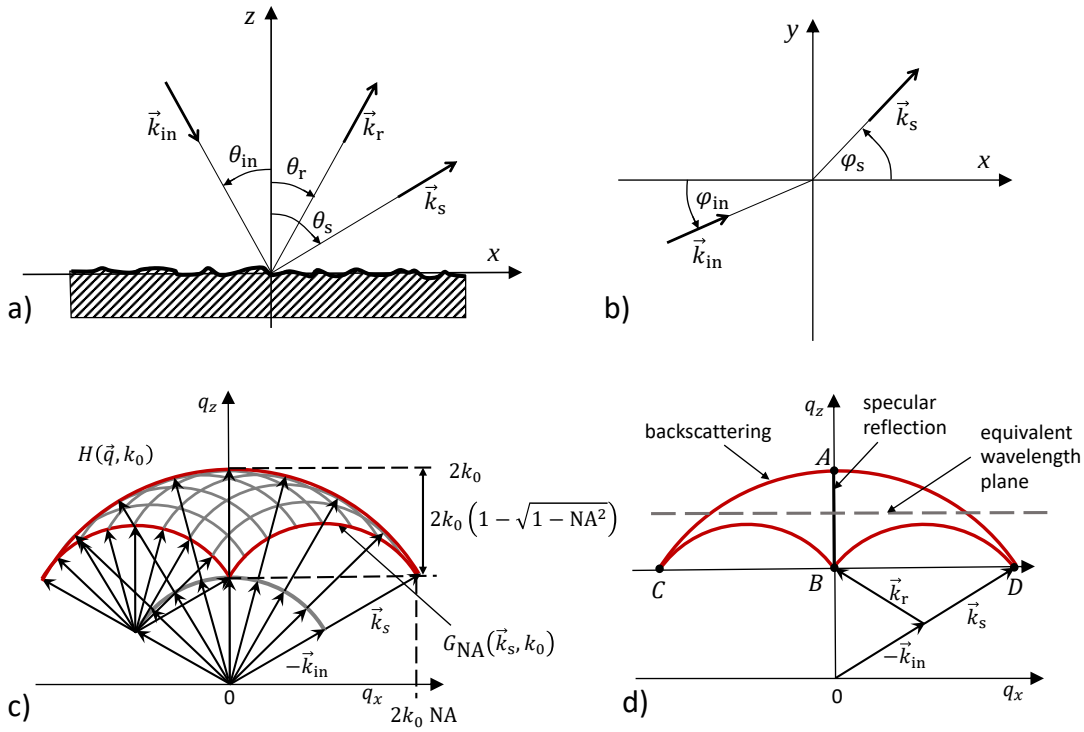

Figure 2. a) Incident, reflected and scattered wave vectors in the xz-plane; b) projections of incident and scattered wave vectors in the xy plane; c) construction of the Ewald sphere in the spatial frequency domain corresponding to a conventional microscope, ($G_{NA}(\vec{k}_s, k_0)$ indicates the transfer function with plane wave illumination under the angle θ_{in}, $H(\vec{q}, k_0)$ corresponds to the transfer function taking all angles of incidence and scattering into account); d) Ewald sphere construction showing the specular reflection between point A and B; the points C and D indicate the positions related to the maximum angles of backscattered scattered and incident light $\theta_s = \mp\theta_{max}$ and $\theta_{in} = \pm\theta_{max}$. (Figure taken from Lehmann et al.[28])

The intensity distribution in the spatial frequency domain is determined by the measured structure and, therefore, by the scattered and reflected light components. Depending on the direction of the corresponding wave vectors, the distribution of the transfer function results in the area marked in red. The part related to the specular reflection is located on the q_z axis between points A and B. The highest spatial frequency image components can be found at points C and D, which indicate the lateral resolution limit of the imaging system. When imaging a laterally extended periodic structure with the period length Λ, the position of the diffraction order on the q_x axis (or q_y axis, respectively) under plane wave illumination results from the equation[32]

$$\theta_{s,n} = \arcsin\left(\frac{n\lambda}{\Lambda} + \sin\theta_{in}\right), \tag{4}$$

which leads to

$$k_0(\sin\theta_{s,n} - \sin\theta_{in}) = q_{x,n} = \frac{2\pi n}{\Lambda}, \tag{5}$$

where n denotes the diffraction order.

4. ANALYSIS OF INTERFEROMETRIC MEASUREMENT DATA

The measurement data, which are to be analyzed in the following, are obtained with the Linnik interferometer (NA = 0.9, 100x magnification) described in chapter 2 with additional microspheres on the measured surface as

a near-field support. First, the analysis of the measurement data of a structure with a period length of 230 nm is presented. The measurement object is a Linewidth/Pitch Standard manufactured by supracon.[33] Further, 3D spatial frequency distributions resulting from measurement data of a Blu-ray Disc are shown. The measuring object is illuminated in a selective manner by means of the DMD used in the beam path in order to illuminate only those areas of the field of view, where a microsphere is located. Hence, interferograms are only obtained for these illuminated areas and reflections from the rest of the field of view are suppressed. Furthermore, certain sections of the interferograms are windowed by a blackman window in order to eliminate interfering reflections from the surface of the microsphere.

We already demonstrated that, when comparing measurement results with and without a microsphere in the spatial frequency domain, a shift of the image information towards lower values on the q_x or q_y axis, i.e. towards lower transverse spatial frequencies can be observed.[29] This was shown by means of measurements of the laterally extended structure of a Blu-ray Disc. With the help of microspheres in the near field, an effectively enlarged numerical aperture appears. The results of an improved data analysis presented in the following further underline this observation.

The interferometric measurement data analysis presented in Figure 3 is based on a grating structure with a period of 230 nm. The results of phase analysis of these data were already published[34] and show that this structure can be resolved by means of the near-field support by microspheres. Therefore, a more in-depth analysis of the measurement data in the spatial frequency domain is of particular interest. Figure 3a) shows a cross section of the interference image stack through the microsphere and in Figure 3b) the phase evaluation result of the measurement data in the profile section of the topography is depicted. Figure 3c) displays the magnitude spectrum of the measurement data in the spatial frequency domain, where the limitation is given by the boundaries of the Ewald sphere explained in chapter 3. It can be pointed out that a clear analysis of the data is difficult due to the disturbing reflections on the spherical surface as well as the influence of other interferences in the cross section. In order to achieve a clearer analysis of the effects of the microsphere on the imaging behavior and the transfer function, the data was windowed in both, the y and z direction using a Blackman window and then transferred to the spatial frequency space to determine the resulting transfer function of the optical system including the microsphere. The result can be seen in Figure 3c).

The results of phase analysis of the measured data in 3b) show that the grating structure with $\Lambda = 230$ nm period length is magnified by the imaging process through the microsphere to a period length of 325 nm, i.e. the magnification is approximately $M = 1.4$. On the q_y axis this leads to the values $q_{y,s} = 2\pi/(M\,\Lambda) = \pm 19.3\ \mu\text{m}^{-1}$. While in Figure 3c) the proportions in the magnitude spectrum at these positions do not have enough intensity to be visible in relation to the intensity of the disturbing reflections and other interferences in the cross-section of the measurement data, in Figure 3d) after windowing of the data it is possible to obtain the corresponding frequency components at the expected positions in the spatial frequency domain (see white markings).

In order to gain further insight into the benefits of microsphere assisted measurements combined with windowing of the data, measurements of a Blu-ray Disc using SiO_2 microspheres (diameter $d = 15\ \mu\text{m}$) have been carried out. The results are compared to those using selective circular and annular illumination of the area in the field of view covered by microspheres and thus improving the measurement data already during the measurement process and not only in the subsequent signal processing. The DMD used in the illumination beam path enables to keep certain areas of the measurement field dark. Figure 4 shows the comparison of the measurement data and the associated transfer behavior in the spatial frequency domain for different data windowing as well as for different illumination cases. The data was either not windowed at all, only in the direction of the z/y-axis or with respect to both, the y and the z axis with an adapted Blackman window. The width of the Blackman window in y-direction is chosen such that the regions in the field of view, which were not covered by the microsphere, are eliminated due multiplication with zero. In z-direction the Blackman window preselects those sections of the sampled interference signals, which belong to the surface structure imaged through the microsphere, thus eliminating reflections from the top surface of the microsphere. With respect to the illumination the cases of a complete bright-field illumination (Fig. 4a)-e)), a circular illumination of the whole area covered by the micro-sphere (Fig. 4f)-j)) and an annular illumination (Fig. 4k)-o)) of the outer region of the microsphere are analyzed and compared.

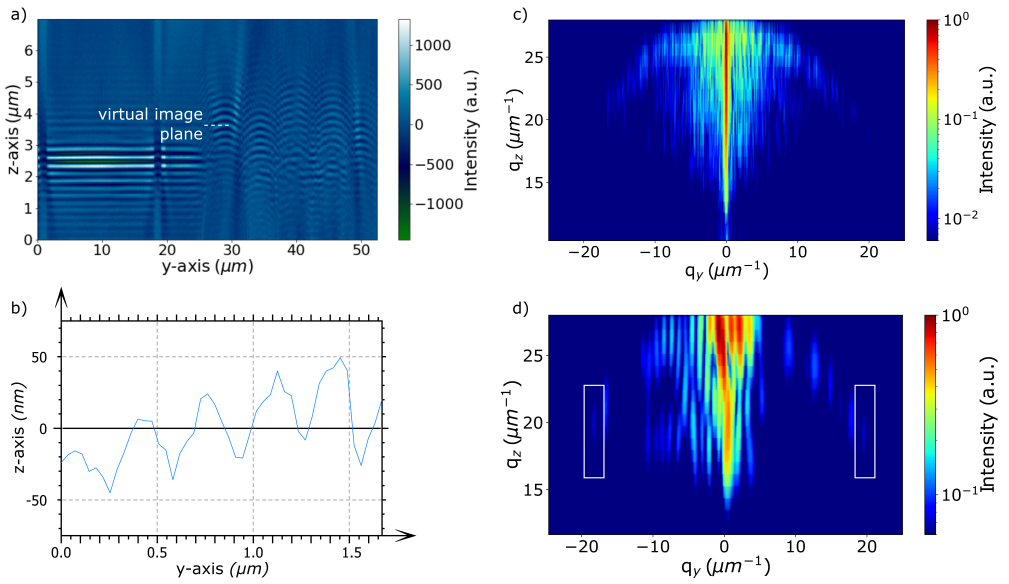

Figure 3. Measurement data of a rectangular periodic grating structure with 230 nm period and 30 nm height difference and the corresponding intensity distributions in the spatial frequency domain. a) interference image stack in the cross section of the microsphere placed on the structure; b) cross section of the phase evaluation result of the topography obtained from the measurement data; c) $q_y q_z$ cross section of the intensity distribution of the interference image stack in the spatial frequency domain; d) $q_y q_z$ cross section of the intensity distribution of the interference image stack after the measurement data was windowed in z and y direction by a Blackman window function.

When considering the magnitude spectrum of the measurement data without selective illumination, in Figure 4b) at $q_y = \pm 20\,\mu\text{m}^{-1}$ the components that are induced by the imaging of the Blu-ray Disc without microsphere support appear in the spatial frequency domain (marked in white, corresponding to the period length of $\Lambda_b = 320\,\text{nm}$ of a Blu-ray Disc[29,35]). In order to analyze the imaging process affected by microspheres, however, these spectral components are not desired and, therefore, circular and annular illumination are used. Both kinds of selective illumination achieve that these components are no longer present in the magnitude spectrum (compare Fig. 4g) and l)). The same effect can be reached by windowing the interferometric measurement data in the direction of the y-axis with a Blackman window function (Fig. 4c)). This shows first of all that windowing in the y direction only leads to more significant magnitude spectra in the spatial frequency domain if additional interferometric measurement data originating from outside the microsphere contribute to the spatial frequency domain representation of the measured image stack and can thus be eliminated.

The windowing of the measurement data in the z-direction shows an elongation of the Ewald spheres in the q_z-direction. Nevertheless, it can be observed that the windowing of the data clearly enhances the frequency components that belong to the topography of the Blu-ray Disc structure enlarged by the microsphere. As we have have already shown,[29] the measurement of the Blu-ray Disc structure in the given experimental environment leads to an additional magnification by the microsphere of 1.4 and thus to spatial frequency components at $q_y = 14\,\mu\text{m}^{-1}$. This is especially evident in 4e) as well as i) and n). These results reveal that microspheres applied in the nearfield influence the position of diffraction maxima of non-zero order in the $\vec{q}$-space. Relevant image information for reconstructing lateral grating structures is shifted to lower values on the $q_{x/y}$-axis and therefore leads to an effective enlargement of the Numerical Aperture and a different transfer behavior of the System. Comparing circular and annular illumination of the microsphere, in the results achieved with the annular illumination the first order diffraction maxima of the Blu-ray structure are less blurred and thus a better reconstruction of the corresponding surface profiles is expected.

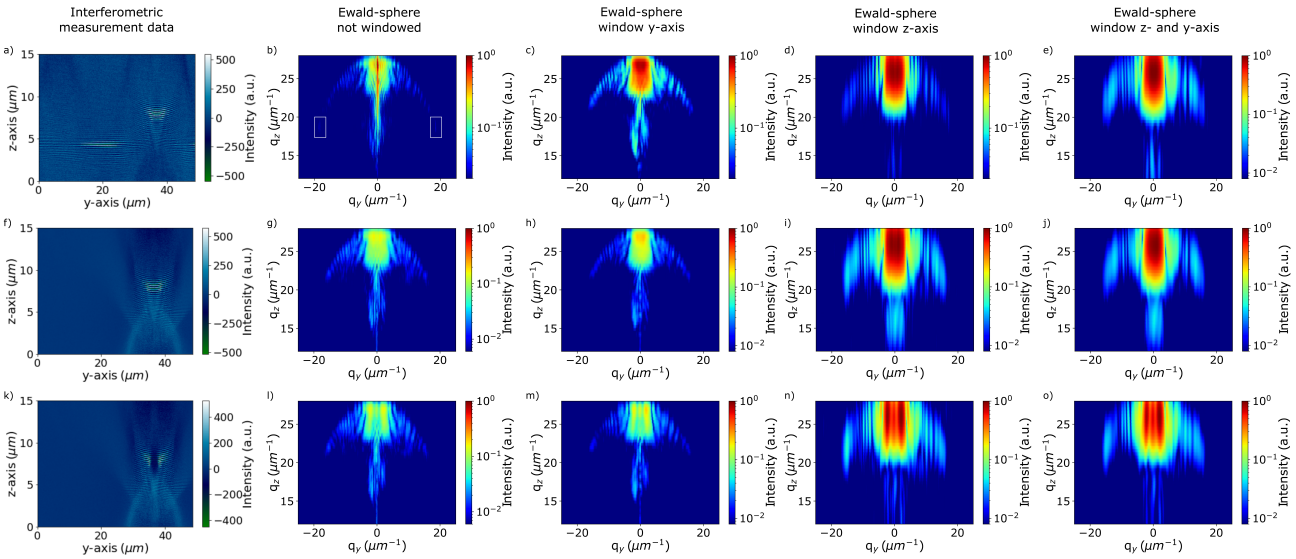

Figure 4. All measurement data depicted in this figure shows data sets obtained with a microsphere (SiO_2, diameter 15 µm) on a Blu-ray Disc. As indicated above the subfigures, interferometric measurement data are shown with their corresponding representation in the spatial frequency domain. The data is windowed in different manners as indicated. a)-e) data set obtained with bright-field illumination, f)-j) data obtained with circular illumination of the microsphere, k)-o) annular illumination.

5. CONCLUSION

In this contribution experimental results and the corresponding analysis in the 3D spatial frequency domain of microsphere-assisted interference microscopy are presented. Both, the measurement data of a calibration grating structure with a period length of 230 nm and a Blu-ray Disc structure of 320 nm period are examined in the spatial frequency domain. Furthermore, the effects of both, selective illumination and adaptive windowing of the measurement data in the signal analysis step, are investigated. This investigation is intended to find out, to what extent manipulation of the measurement data during the measurement process and in the analysis process can contribute to improve the measurement results and the understanding of the imaging processes during the measurement through microspheres applied in the near field of the object's surface. It has been shown that both, selective circular or annular lighting and windowing of the measurement data in the direction of the x/y-axis have a similar effect on the measurement data and ensure that the frequency components of structures located in the field of view in the vicinity of the microsphere no longer contribute to the magnitude spectrum in the 3D spatial frequency domain and therefore no longer disturb the topography reconstruction.

The windowing of the measurement data in the direction of the scan axis z leads to an elongation of the Ewald sphere in q_z-direction, but makes the frequency components along the $q_{x/y}$ axis, which are relevant for the analysis of the transfer behavior, more prominent.

Analyzing the measurement data emphasizes the role of the shift of the lateral spatial frequency components caused by the microsphere-induced additional magnification of the structures shown. Therefore, the effect that arises from the near-field support of the microspheres can be viewed as an effective enlargement of the numerical aperture of the optical system. High-frequency components of laterally extended structures are shifted to lower spatial frequencies by the enlargement and thus are relocated in the spatial frequency domain to portions of the 3D transfer function that contribute to the image formation by the optical system. In further studies the influences of selective illumination as well as windowing of interferometric measurement data on the reconstruction of the object's 3D topography will be discussed.

ACKNOWLEDGMENTS

This work is funded by the DFG (German Research Foundation) under the project number LE992/15-1.

REFERENCES

[1] Tereschenko, S., *Digitale Analyse periodischer und transienter Messsignale anhand von Beispielen aus der optischen Präzisionsmesstechnik*, PhD thesis, Universität Kassel (2018).

[2] Hecht, E., [*Optik*], Oldenbourg (2001).

[3] Wang, Z., Guo, W., Li, L., Luk, B., Khan, A., and Liu, Z., "Supplementary Information Optical virtual imaging at 50 nm lateral resolution with a white light nanoscope," *Nature communications* **2**, 1–7 (2011).

[4] Darafsheh, A., Walsh, G. F., Dal Negro, L., and Astratov, V. N., "Optical super-resolution by high-index liquid-immersed microspheres," *Applied Physics Letters* **101**(14), 141128 (2012).

[5] Darafsheh, A., Limberopoulos, N. I., Derov, J. S., Walker, D. E., and Astratov, V. N., "Advantages of microsphere-assisted super-resolution imaging technique over solid immersion lens and confocal microscopies," *Applied Physics Letters* **104**(6) (2014).

[6] Li, L., Guo, W., Yan, Y., Lee, S., and Wang, T., "Label-free super-resolution imaging of adenoviruses by submerged microsphere optical nanoscopy," *Light: Science and Applications* **2**(SEPTEMBER), 1–9 (2013).

[7] Yan, Y., Li, L., Feng, C., Guo, W., Lee, S., and Hong, M., "Microsphere-Coupled Scanning Laser Confocal Nanoscope for Sub-Diffraction-Limited Imaging at 25 nm Lateral Resolution in the Visible Spectrum," *ACS Nano* **8**, 1809–1816 (feb 2014).

[8] Montgomery, P., Lecler, S., Perrin, S., Li, H., and Leong-Hoi, A., "Illumination conditions in microsphere-assisted microscopy," *Journal of Microscopy* **274**(1), 69–75 (2019).

[9] Perrin, S., Li, H., Badu, K., Comparon, T., Quaranta, G., Messaddeq, N., Lemercier, N., Montgomery, P., Vonesch, J. L., and Lecler, S., "Transmission Microsphere-Assisted Dark-Field Microscopy," *Physica Status Solidi - Rapid Research Letters* **13**(2), 1–4 (2019).

[10] Wang, F., Liu, L., Yu, P., Liu, Z., Yu, H., Wang, Y., and Li, W. J., "Three-dimensional super-resolution morphology by near-field assisted white-light interferometry," *Scientific Reports* **6**(April), 24703 (2016).

[11] Perrin, S., Leong-Hoï, A., Lecler, S., Pfeiffer, P., Kassamakov, I., Nolvi, A., Hæggström, E., and Montgomery, P., "Microsphere-assisted phase-shifting profilometry," *Applied Optics* **56**(25), 7249–7255 (2017).

[12] Leong-Hoi, A., Hairaye, C., Perrin, S., Lecler, S., Pfeiffer, P., and Montgomery, P., "High Resolution Microsphere-Assisted Interference Microscopy for 3D Characterization of Nanomaterials," *Physica Status Solidi (A) Applications and Materials Science* **215**(6), 1–7 (2018).

[13] Montgomery, P. C., Lecler, S., Leong-hoï, A., Perrin, S., and Pfeiffer, P., "Sub-diffraction surface topography measurement using a microsphere- assisted Linnik interferometer," *Proceedings of SPIE - The International Society for Optical Engineering* **10329**(33), 1–10 (2017).

[14] Montgomery, P., Lecler, S., Leong-Hoi, A., and Pfeiffer, P., "3D nano surface profilometry by combining the photonic nanojet with interferometry," *Journal of Physics: Conf. Series* **794**(1), 012006 (2017).

[15] Kassamakov, I., Lecler, S., Nolvi, A., Leong-Hoï, A., Montgomery, P., and Hæggström, E., "3D Super-Resolution Optical Profiling Using Microsphere Enhanced Mirau Interferometry," *Scientific Reports* **7**(1), 1–7 (2017).

[16] Yang, H., Trouillon, R., Huszka, G., and Gijs, M. A., "Super-Resolution Imaging of a Dielectric Microsphere Is Governed by the Waist of Its Photonic Nanojet," *Nano Letters* **16**(8), 4862–4870 (2016).

[17] Heifertz, A., Kong, S.-C., Sahakian, A. V., Taflove, A., and Backman, V., "Photonic Nanojets," *Comput Theor Nanosci.* **6**(9), 1979–1992 (2009).

[18] Rockstuhl, C., Kim, M.-S., Herzig, H. P., Scharf, T., and Mühlig, S., "Engineering photonic nanojets," *Optics Express* **19**(11), 10206 (2011).

[19] Kim, M. S., Scharf, T., Mühlig, S., Rockstuhl, C., and Herzig, H. P., "Gouy phase anomaly in photonic nanojets," *Applied Physics Letters* **98**(19), 2–5 (2011).

[20] Zhou, S., Deng, Y., Zhou, W., Yu, M., Urbach, H. P., and Wu, Y., "Effects of whispering gallery mode in microsphere super-resolution imaging," *Applied Physics B: Lasers and Optics* **123**(9), 1–9 (2017).

[21] Wu, M. X., Huang, B. J., Chen, R., Yang, Y., Wu, J. F., Ji, R., Chen, X. D., and Hong, M. H., "Modulation of photonic nanojets generated by microspheres decorated with concentric rings," *Optics Express* **23**(15), 20096 (2015).

[22] Sheppard, C. J., Connolly, T. J., and Gu, M., "Imaging and reconstruction for rough surface scattering in the kirchhoff approximation by confocal microscopy," *Journal of Modern Optics* **40**(12), 2407–2421 (1993).

[23] Quartel, J. C. and Sheppard, C. J., "A surface reconstruction algorithm based on confocal interferometric profiling," *Journal of Modern Optics* **43**(3), 591–605 (1996).
[24] Quartel, J. C. and Sheppard, C. J., "Surface reconstruction using an algorithm based on confocal imaging," *Journal of Modern Optics* **43**(3), 469–486 (1996).
[25] Coupland, J. M. and Lobera, J., "Holography, tomography and 3D microscopy as linear filtering operations," *Measurement Science and Technology* **19**(7) (2008).
[26] Coupland, J., Mandal, R., Palodhi, K., and Leach, R., "Coherence scanning interferometry: Linear theory of surface measurement," *Applied Optics* **52**(16), 3662–3670 (2013).
[27] Su, R., Coupland, J., Sheppard, C., and Leach, R., "Scattering and three-dimensional imaging in surface topography measuring interference microscopy," *Journal of the Optical Society of America A* **38**(2), A27 (2021).
[28] Lehmann, P., Künne, M., and Pahl, T., "Analysis of interference microscopy in the spatial frequency domain," *Journal of Physics: Photonics* **3**(014006), 1–17 (2021).
[29] Hüser, L. and Lehmann, P., "Microsphere-assisted interference microscopy for resolution enhancement," *Technisches Messen* **88**(5), 311–318 (2021).
[30] Beckmann, P. and Spizzichino, A., "The scattering of electromagnetic waves from rough surfaces," *Norwood: Artech House Inc.* (1987).
[31] Su, R., Thomas, M., Liu, M., Drs, J., Bellouard, Y., Pruss, C., Coupland, J., and Leach, R., "Lens aberration compensation in interference microscopy," *Optics and Lasers in Engineering* **128**(November 2019), 106015 (2020).
[32] Xie, W., *Transfer characteristics of white light interferometers and confocal microscopes*, PhD thesis, Universität Kassel (2017).
[33] Huebner, U., Morgenroth, W., Boucher, R., Meyer, M., Mirandé, W., Buhr, E., Ehret, G., Dai, G., Dziomba, T., Hild, R., and Fries, T., "A nanoscale linewidth/pitch standard for high-resolution optical microscopy and other microscopic techniques," *Measurement Science and Technology* **18**(2), 422–429 (2007).
[34] Hüser, L. and Lehmann, P., "Microsphere assisted interferometry with high numerical apertures for 3D topography measurements," *Applied Optics* **59**(6), 1695–1702 (2020).
[35] Hagemeier, S., Schake, M., and Lehmann, P., "Sensor characterization by comparative measurements using a multi-sensor measuring system," *Journal of Sensors and Sensor Systems* **8**(1), 111–121 (2019).

L. Hüser, P. Lehmann, "Analysis of resolution enhancement through microsphere-assisted interferometry in the 3D spatial frequency domain" SPIE Proceedings 11782, Optical Measurement Systems for Industrial Inspection XII, 117820R, (June 20, 2021).

https://doi.org/10.1117/12.2593296